THE JOURNAL OF BIOLOGICAL CHEMISTRY VOL. 291, NO. 48, pp. 25019–25031, November 25, 2016
Published in the U.S.A.

# Hydrogen Bonding to the Substrate Is Not Required for Rieske Iron-Sulfur Protein Docking to the Quinol Oxidation Site of Complex III*

Received for publication, July 1, 2016, and in revised form, October 5, 2016 Published, JBC Papers in Press, October 7, 2016, DOI 10.1074/jbc.M116.744391

**Lothar Esser[‡1], Fei Zhou[‡1], Yihui Zhou[‡§], Yumei Xiao[‡§], Wai-kwan Tang[‡], Chang-An Yu[¶], Zhaohai Qin[§], and Di Xia[‡2]**

*From the [‡]Laboratory of Cell Biology, Center for Cancer Research, National Cancer Institute, National Institutes of Health, Bethesda, Maryland 20892, the [§]College of Science, China Agricultural University, Beijing 100193, China, and the [¶]Department of Biochemistry and Molecular Biology, Oklahoma State University, Stillwater, Oklahoma 74078*

**Edited by Norma Allewell**

**Complex III or the cytochrome (cyt) $bc_1$ complex constitutes an integral part of the respiratory chain of most aerobic organisms and of the photosynthetic apparatus of anoxygenic purple bacteria. The function of cyt $bc_1$ is to couple the reaction of electron transfer from ubiquinol to cytochrome *c* to proton pumping across the membrane. Mechanistically, the electron transfer reaction requires docking of its Rieske iron-sulfur protein (ISP) subunit to the quinol oxidation site ($Q_P$) of the complex. Formation of an H-bond between the ISP and the bound substrate was proposed to mediate the docking. Here we show that the binding of oxazolidinedione-type inhibitors famoxadone, jg144, and fenamidone induces docking of the ISP to the $Q_P$ site in the absence of the H-bond formation both in mitochondrial and bacterial cyt $bc_1$ complexes, demonstrating that ISP docking is independent of the proposed direct ISP-inhibitor interaction. The binding of oxazolidinedione-type inhibitors to cyt $bc_1$ of different species reveals a toxophore that appears to interact optimally with residues in the $Q_P$ site. The effect of modifications or additions to the toxophore on the binding to cyt $bc_1$ from different species could not be predicted from structure-based sequence alignments, as demonstrated by the altered binding mode of famoxadone to bacterial cyt $bc_1$.**

The ubiquinol-cytochrome *c* oxidoreductase, also known as complex III of mitochondrial respiratory chain or cytochrome (cyt)[3] $bc_1$ complex, catalyzes the reaction of electron transfer (ET) from ubiquinol ($QH_2$) to cyt *c* and concomitantly translocates protons across the inner membrane of mitochondria or the plasma membrane of photosynthetic purple bacteria, contributing to a cross-membrane potential important for cellular function (1, 2). Although catalyzing the same enzymatic reaction, cyt $bc_1$ complexes isolated from different organisms have very different subunit compositions. Prokaryotic $bc_1$ complexes often consist of 3–4 subunits, whereas mitochondrial enzymes have 10–11 different subunits (1). Nevertheless, only three subunits are essential for the ET function (Fig. 1*A*): cyt *b*, cyt $c_1$, and the Rieske iron-sulfur protein (ISP) (3). The cyt *b* subunit contains two *b*-type hemes, $b_L$ and $b_H$, for the low and high potential hemes, respectively, and is entirely embedded in the membrane with eight transmembrane (TM) helices (4). The cyt $c_1$ subunit, anchored to the membrane by a single TM helix, has a *c*-type heme covalently attached to its active domain that is located in the intermembrane space of mitochondria or periplasm in bacteria. The ISP subunit features an integrated 2Fe-2S cluster in its extrinsic domain (ISP-ED) that is on the same side as the cyt $c_1$ subunit and also anchored to the membrane by a helix.

The ET-coupled proton translocation function, as modeled by the Q-cycle mechanism (Fig. 1*B*), requires two active sites: a $QH_2$ oxidation ($Q_P$) site and a ubiquinone (Q) reduction ($Q_N$) site (5–7), which were shown to exist by crystal structures of mitochondrial and bacterial $bc_1$ complexes in complexes with various $bc_1$-specific inhibitors (4, 8–12). A characteristic feature of the Q-cycle mechanism is the bifurcated ET pathway at the $Q_P$ site, in which the two electrons of the substrate $QH_2$ take two separate routes (Fig. 1*B*): one takes a high potential route going from ISP to cyt $c_1$ and to substrate cyt *c*, and the other follows the low potential route traveling to the $b_L$ and $b_H$ hemes sequentially, ending in ubiquinone/ubisemiquinone bound at the $Q_N$ site. Strikingly, structural studies of bovine mitochondrial cyt $bc_1$ (*Btbc*$_1$) in complex with various respiratory inhibitors revealed the inhibitor-type dependent conformation switch of ISP-ED. This observation not only suggested a mechanism for the $QH_2$ oxidation at the $Q_P$ site but also offered a

* This work was supported by the Intramural Research Program of the National Institutes of Health, National Cancer Institute, Center for Cancer Research, and a grant from the National Basic Research Science Foundation of China (2010CB126100) (to Z. Q.). The authors declare that they have no conflicts of interest with the contents of this article. The content is solely the responsibility of the authors and does not necessarily represent the official views of the National Institutes of Health.

*The atomic coordinates and structure factors (codes 5KKZ, 5KLI, and 5KLV) have been deposited in the Protein Data Bank (http://wwpdb.org/).*

[1] Both authors contributed equally to this work.

[2] To whom correspondence should be addressed. E-mail: xiad@mail.nih.gov.

[3] The abbreviations used are: cyt, cytochrome; Ar-Ar, aromatic-aromatic interaction; $bc_1$, cytochrome $bc_1$; $b_H$, high potential heme *b*; $b_L$, low potential heme *b*; *Btbc*$_1$, *Bos taurus* mitochondrial $bc_1$; ET, electron transfer; famoxadone, 5-methyl-5-(4-phenoxy-phenyl)-3-phenylamino-2,4-oxazolidinedione; fenamidone, (5*S*)-5-methyl-2-(methylsulfanyl)-5-phenyl-3-(phenylamino)-3,5-dihydro-4*H*-imidazol-4-one; *Ggbc*$_1$, *Gallus gallus* mitochondrial $bc_1$; ISP, iron-sulfur protein; ISP-ED, extrinsic domain of ISP; jg144, 5-methyl-5-(4,6-difluorophenyl)-3-phenylamino-2,4-oxazolidinedione; NCS, non-crystallographic symmetry; $Q_P$, ubiquinol oxidation; $Q_N$, ubiquinone reduction; RMS, root mean square; *Rsbc*$_1$, $bc_1$ from photosynthetic bacterium *R. sphaeroides*; TM, transmembrane; PDB, Protein Data Bank; DDM, dodecyl-D-maltopyranoside; β-OG, β octyl glucoside.

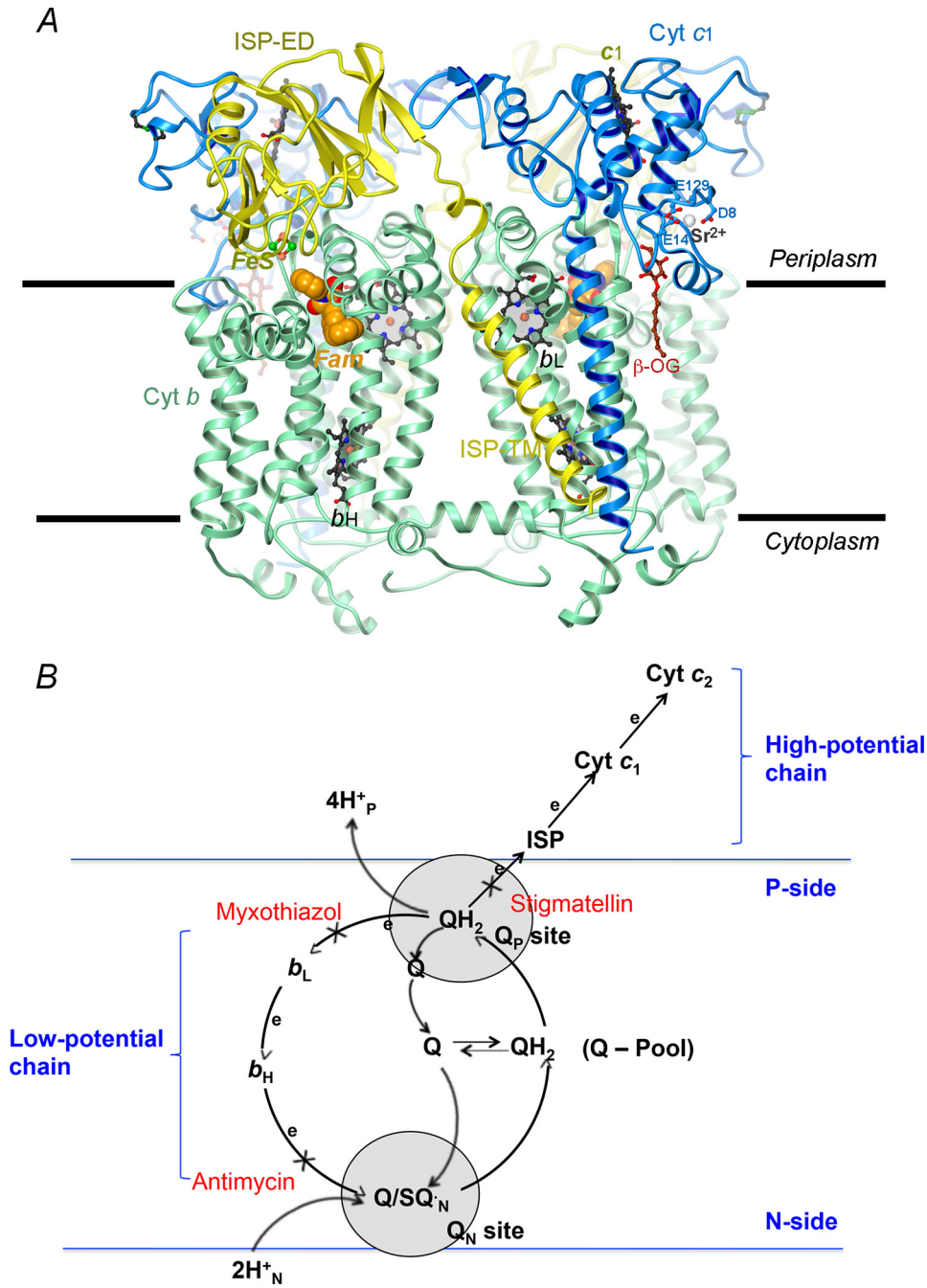


FIGURE 1. **Structure and mechanism of cyt $bc_1$ complex.** *A*, ribbon representation of the structure of dimeric cyt $bc_1$ in complex with famoxadone from photosynthetic bacterium *R. sphaeroides*. The cyt *b* subunit is shown in *green*, the cyt $c_1$ is in *blue*, and ISP is in *yellow*. Heme groups are shown as the ball and stick models with carbon in *black*, nitrogen in *blue*, and oxygen in *red*; they are labeled in *black* as $b_H$, $b_L$, and $c_1$, respectively. The iron-sulfur cluster (*FeS*) of ISP is shown as *spheres* with Fe in *orange-brown* and S in *green*. The two parallel *horizontal lines* represent the cytoplasm membrane bilayer. The bound famoxadone (*Fam*) at the $Q_P$ site is shown as the CPK model with carbon in *orange*, oxygen in *red*, and nitrogen in *blue*. One detergent molecule (*β*-OG) bound at cyt $c_1$ is drawn as a *brown/red* ball and stick model. A bound strontium ion ($Sr^{2+}$) bound to cyt $c_1$ is also shown together with its amino acid ligands $Asp^8$, $Glu^{14}$, and $Glu^{129}$ in the stick models. *B*, Q-cycle mechanism. The cyt $bc_1$ consists of two reaction sites: $Q_P$ and $Q_N$ sites. The $Q_P$ site is near the P side, where the two electrons of $QH_2$ diverge. The first electron goes to the high potential chain via the ISP and cyt $c_1$, ending in cyt $c_2$ (cyt *c* in mitochondrial cyt $bc_1$), which can be interrupted by stigmatellin. The second electron enters the low potential chain via hemes $b_L$ and $b_H$, end in substrate Q or radical $Q^{\cdot}$ bound at the $Q_N$ site. The low potential path can be inhibited by myxothiazol at the $Q_P$ site and antimycin at the $Q_N$ site.

means for inhibitor classification (13–15). Thus, inhibitors that immobilize the ISP-ED to the $Q_P$ site are called $P_f$-type inhibitors, and those that mobilize it are termed $P_m$-type inhibitors (13).

High resolution structural studies of cyt $bc_1$ have so far failed to show the binding of substrate $QH_2$ at the $Q_P$ site. Studies of cyt $bc_1$ in the presence of inhibitors that are substrate $QH_2$ homologs such as stigmatellin (4, 11–13, 16, 17), 3-Undecyl-2-hydroxydioxobenzothiazol (13), 5-n-heptyl-6-hydroxy-4,7-dioxobenzothiazole (18), and 2-nonyl-4-hydroxyquinoline N-oxide (13) revealed conformational immobilization or docking of the ISP-ED to the $Q_P$ site and a hydrogen bond (H-bond, 2.8 –

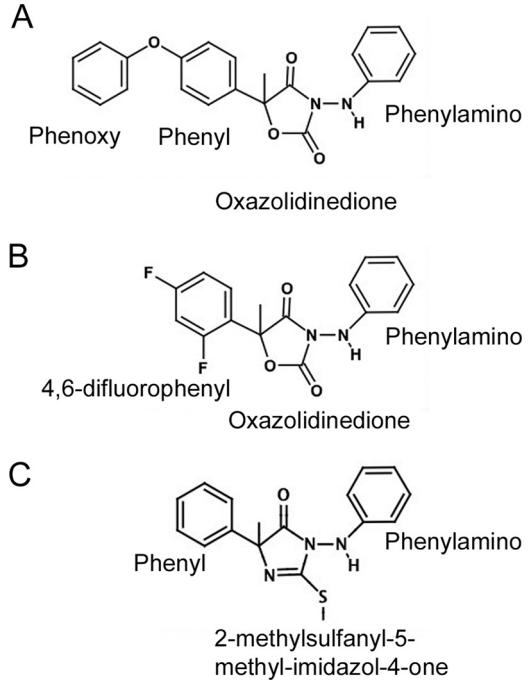


FIGURE 2. **Chemical structures of famoxadone (*A*), jg144 (*B*), and fenamidone (*C*).**

3.4 Å depending on the structure) between the histidine ligand to the 2Fe-2S cluster of ISP ($His^{141}$, bovine sequence) and oxygen moieties of the inhibitor, leading to the proposal that docking of the ISP-ED to the $Q_P$ site is likely the consequence of this H-bond (11, 19, 20). Despite evidence that suggests the docking of the ISP-ED to the $Q_P$ site may be independent of the H-bond (21), systematic study is lacking.

The dire consequence of obstructing cellular respiration has made cyt $bc_1$ one of the most frequent targets of antibiotics. However, allelopathic inhibition has been observed as a strategy employed by many organisms to gain survival advantage (22). Consequently, toxin-producing organisms are intrinsically resistant to their own toxin. Although many mechanisms may be at work to render this intrinsic resistance, changes in target structures by amino acid substitutions are believed to contribute significantly to the phenomenon, leading to amino acid sequence diversification at the site of inhibition across organisms. Inhibitors of $bc_1$ have been used not only for the purpose of disease control but also in studies of the mechanisms of $bc_1$ function, inhibition, and resistance (13, 14, 23–28). Famoxadone (5-methyl-5-(4-phenoxy-phenyl)-3-phenylamino-2,4-oxazolidinedione) (Fig. 2*A*) is an oxazolidinedione-type $Q_P$ site inhibitor (29). It has reportedly displayed various $IC_{50}$ values for submitochondrial particles from different species (30). However, evidence is mounting that some fungal species are intrinsically more resistant (30, 31), and field applications of famoxadone for fungal disease control have led to rapid development of resistance that renders the inhibitor ineffective (32–34). How inhibitors such as famoxadone react to fluidity in its binding environment has not been fully explored experimentally, let alone understood.

It is known that the ET between the ISP and cyt $c_1$ requires movement of the ISP-ED, which could be controlled, as we proposed earlier (14), by the bimodal conformation switch of the ISP-ED. Thus, the question regarding the involvement of the H-bond in this control process needs to be addressed. In the present study, we used three oxazolidinedione-type inhibitors to form complexes with either mitochondrial or bacterial cyt $bc_1$ or both and showed that all three inhibitors can induce docking of the ISP-ED at the $Q_P$ site without forming a direct H-bond with the ISP, which is consistent with the notion that the ISP conformation switch does not require a direct H-bond. We established the structural basis for the toxophore of oxazolidinedione-type inhibitors and showed the effect of alterations to the toxophore on inhibitor binding to the cyt $bc_1$, both structurally and biochemically. These observations have strong implications concerning the development of drugs that are designed to target a broad spectrum of pathogens.

## Results

*Differential Inhibition of Mitochondrial and Bacterial cyt $bc_1$ Complexes by Famoxadone*—Previously, we reported that binding of famoxadone to $Btbc_1$ induces docking of the ISP to the $Q_P$ site (21). Unlike other $Q_P$ site inhibitors such as stigmatellin and 3-Undecyl-2-hydroxydioxobenzothiazol, famoxadone does not make a direct H-bond with the ISP-ED because the shortest distance between $His^{141}$ of the ISP and the phenylamino moiety of famoxadone is 6.1 Å (Fig. 3*A*). However, whether the fixation of the ISP-ED by famoxadone binding can be interpreted as part of the Q-cycle mechanism remains unclear. Thus, to understand this phenomenon, one would have to investigate the effect of famoxadone on cyt $bc_1$ of other organisms, which are evolutionarily remote from mammals or yeast, such as bacteria. Doubts that the capture of the ISP-ED induced by famoxadone binding is indeed part of a conserved mechanism were initially cast by the observation that the experimentally determined $IC_{50}$ values of 1.4 and 418 nM of isolated cyt $bc_1$ from photosynthetic bacterium *Rhodobacter sphaeroides* ($Rsbc_1$) and mitochondrial cyt $bc_1$ ($Btbc_1$), respectively, differ by a factor of nearly 300 (Fig. 4*A*). Further differences were noticed in the shapes of the inhibition curves for $Rsbc_1$ and $Btbc_1$, suggesting that $Rsbc_1$ might exhibit a different set of binding interactions with famoxadone.

Paradoxically, the difference in $IC_{50}$ values is not supported by the apparent conservation in the $Q_P$ site, because all residues in contact with famoxadone in $Btbc_1$ are conserved, except for two residues: $Phe^{276}$ and $Ala^{277}$ ($Pro^{300}$ and $Phe^{301}$ in $Rsbc_1$, Fig. 5). The closest distances between these two $Btbc_1$ residues and bound famoxadone are 4.53 and 3.72 Å, respectively (Fig. 3*A*). Judging by the alignment between $Btbc_1$ (PDB code 1L0L) and $Rsbc_1$ (PDB code 2FYN) structures, it seems unlikely that these two amino acid substitutions would result in a significant change in the binding of famoxadone, because modeling exercises indicate residue $Phe^{301}$ in $Rsbc_1$ appears to be in a good position to replace the function of $Phe^{276}$ in $Btbc_1$.

*Distinct Conformation of Famoxadone as the $Q_P$ Site Occupant of $Rsbc_1$*—To answer questions about the binding mode of the inhibitor famoxadone and its local and global effect, we determined the crystal structure of $Rsbc_1$ in complex with famoxadone (Fig. 1*A*, Table 1). There are four copies of cyt $bc_1$ in the $Rsbc_1$ crystal per asymmetric unit, each binding one mol-

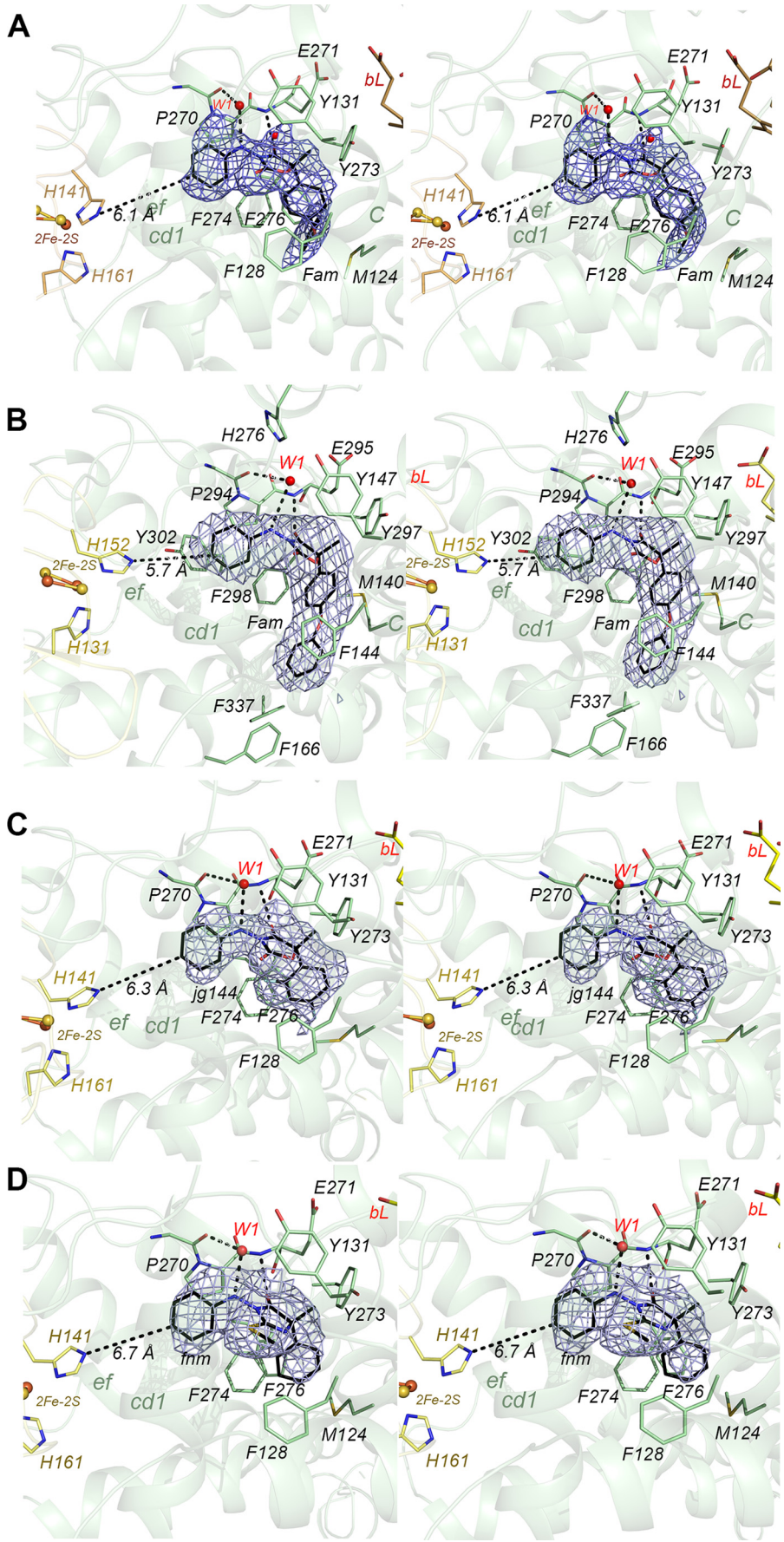
A
E271
bL
W1
Y131
P270
Y273
H141
6.1 Å
ef
F274
F276
C
2Fe-2S
cd1
H161
F128
Fam
M124
B
H276
E295
W1
Y147
bL
P294
Y297
H152
Y302
5.7 Å
2Fe-2S
M140
ef
F298
Fam
cd1
C
H131
F144
F337
F166
C
E271
bL
W1
Y131
P270
Y273
H141
6.3 Å
jg144
ef
cd1
F274
F276
2Fe-2S
F128
H161
D
E271
bL
W1
Y131
P270
Y273
H141
6.7 Å
fnm
ef
2Fe-2S
cd1
F274
F276
M124
F128
H161

ecule of famoxadone. Even though no non-crystallographic symmetry (NCS) restraints were applied to the inhibitor during refinement, the four famoxadone molecules superpose within 0.198 Å root mean square (RMS) deviation, allowing our analysis to focus on just one molecule.

The structure of the *Rsbc*$_1$·famoxadone complex reveals that famoxadone binds in the same location as in *Btbc*$_1$ (Fig. 3*B*). Like *Btbc*$_1$, the chiral environment of the $Q_P$ site of *Rsbc*$_1$ selects the *S*-(−)-isomer of famoxadone for binding. Most importantly for mechanistic implications, the ISP-ED is found docking in the $Q_P$ position, as evidenced by the strong peak of the anomalous difference Fourier density at the location of the 2Fe-2S cluster of ISP. At the same time, residue His$^{152}$ (ligand to the 2Fe-2S cluster in *Rsbc*$_1$ and equivalent of His$^{141}$ of *Btbc*$_1$) has a distance of 5.7 Å to the phenylamino group of famoxadone. This result confirms that recruitment of the ISP to the $Q_P$ site does not depend on the H-bond formation between the ISP-ED and the inhibitor.

As in the *Btbc*$_1$·famoxadone structure, the inhibitor bound to *Rsbc*$_1$ is capable of forming an H-bond between atom O6 and the backbone amide nitrogen atom of Glu$^{295}$ over a distance of 2.69 Å and between atom N1 and the conserved water molecule (W1) (Fig. 3*B*). Unexpectedly, the terminal phenoxy group adopts a position essentially opposite to that found in *Btbc*$_1$·famoxadone, which is quantifiable by a change in torsion angle (C12-C11-O14-C15) from −116° to +145° (Fig. 6*A*). However, this difference in positions of the phenoxy group is consistent with the observation that the residues lining the entrance to the $Q_P$ pocket are quite variable between cyt *b* subunits of different organisms. The adaptation of the terminal phenoxy group to a different environment appears to be based on both exclusion and attraction. The exclusion is caused by the substitution of Ala$^{277}$ of *Btbc*$_1$ with Phe$^{301}$ in *Rsbc*$_1$ (Fig. 5), which would not allow the phenoxy group to be in the same position as in *Btbc*$_1$. Being flexible to swing around, the aromatic phenoxy group of famoxadone finds stabilization by aromatic attractions from Phe$^{166}$, Phe$^{337}$, and Phe$^{144}$ (Figs. 3*B* and 5*A*), which correspond to Ile$^{150}$, Ala$^{295}$, and Phe$^{128}$ in the bovine sequence.

Famoxadone has been noted to prefer aromatic environments (21), which is demonstrated most convincingly by the 13-fold increase in $IC_{50}$ value for the F129L mutation in yeast (30). Thus, the combined effect of the naturally occurring aromatic residues Phe$^{166}$ and Phe$^{337}$ in the cyt *b* subunit of *Rsbc*$_1$ (as opposed to the respective residues Leu$^{150}$ and Ala$^{295}$ in *Btbc*$_1$) might cause the stabilization of famoxadone in the present conformation and explain the difference in $IC_{50}$ values compared with *Btbc*$_1$ (Fig. 4*A*).

Mapping the interactions between $Q_P$ site residues and bound famoxadone, it became immediately apparent that *Rsbc*$_1$ uses an overlapping but non-identical set of residues from *Btbc*$_1$ for famoxadone binding (Fig. 5). Most notably, *Rsbc*$_1$ uses Phe$^{166}$, Met$^{336}$, and Phe$^{337}$ to engage famoxadone, whereas the equivalent residues Leu$^{150}$, Leu$^{294}$, and Ala$^{295}$ in *Btbc*$_1$ remain uninvolved with the inhibitor. Conversely, not all interactions observed in *Btbc*$_1$ are also found in the *Rsbc*$_1$·famoxadone complex, as seen in residues Phe$^{91}$, Tyr$^{95}$, Phe$^{276}$, Ala$^{277}$, and Ile$^{298}$ in *Btbc*$_1$ (Phe$^{105}$, Tyr$^{109}$, Pro$^{300}$, Phe$^{301}$, and Ile$^{340}$ in *Rsbc*$_1$) (Fig. 5). Thus, these structural observations qualitatively explain the differences in $IC_{50}$ values for famoxadone binding to *Btbc*$_1$ and *Rsbc*$_1$, which could not be predicted based on sequence alignment.

*Oxazolidinedione-type Inhibitors Induce Docking of the ISP-ED to the $Q_P$ Site without Direct H-bonding to the ISP and Inhibitor-bound Btbc$_1$ Structures Reveal a Conserved Core-binding Motif*—Superposition of the cyt *b* subunits of *Rsbc*$_1$ and *Btbc*$_1$ complexed with famoxadone shows a good structural alignment of the oxazolidinedione core of famoxadone and its two directly connected aromatic rings (Fig. 6*A*), which raises the question as to whether the difference in binding affinity of famoxadone between *Rsbc*$_1$ and *Btbc*$_1$ is entirely due to the difference in interaction with the terminal phenoxy group. To evaluate the amount of binding energy contributed by various portions of famoxadone other than the phenoxyl group, we measured the binding of two additional oxazolidindione-type compounds, 5-methyl-5-(4,6-difluorophenyl)-3-phenylamino-2,4-oxazolidinedione (jg144) and 5-methyl-2-(methylsulfanyl)-5-phenyl-3-(phenylamino)-3,5-dihydro-4*H*-imidazol-4-one (fenamidone), to both *Btbc*$_1$ and *Rsbc*$_1$ (Fig. 4, *B* and *C*). The chemical structures of jg144 and fenamidone closely resemble that of famoxadone except that they do not have the conformationally flexible terminal phenoxy group (Fig. 2, *B* and *C*). Although jg144 replaces the phenoxy group and the hydrogen atom H9 of famoxadone each with fluorine, fenamidone features a substituted imidazole ring in place of the oxazolidinedione ring.

The $IC_{50}$ values for jg144 inhibition were determined to be 1.1 and 1.2 nM, respectively, for *Rsbc*$_1$ and *Btbc*$_1$ (Fig. 4*B*). Similarly, the $IC_{50}$ values for fenamidone were 3.5 and 8.3 nM, respectively, for *Rsbc*$_1$ and *Btbc*$_1$ (Fig. 4*C*). More importantly, the profiles of the jg144 and fenamidone inhibition curves are very similar regardless of whether they bind to *Rsbc*$_1$ or *Btbc*$_1$, indicating that similar interactions are employed for their binding.

We determined and refined the structure for the complex *Btbc*$_1$·fenamidone at 2.65 Å resolutions (Table 1) and reanalyzed the structure of *Btbc*$_1$·jg144 (PDB code 2FYU) at 2.25 Å resolution. In both cases, their respective ISP-EDs are docked at the $Q_P$ site, as indicated by the high anomalous peak heights of the 2Fe-2S clusters (Table 2). The arrest of the ISP-ED is a

FIGURE 3. **Stereoscopic pairs showing the inhibitor-binding environment of the $Q_P$ site of the cyt *b* subunits of mitochondrial and bacterial *$bc_1$*.** *A*, famoxadone (*Fam*) in *Btbc*$_1$ (PDB code 1L0L). *B*, famoxoadone in *Rsbc*$_1$. *C*, jg144 in *Btbc*$_1$. *D*, fenamidone (*fmn*) in *Btbc*$_1$. The inhibitor binding environment of the $Q_P$ site in the cyt *bc*$_1$ is illustrated as a ribbon model with the cyt *b* subunit in *green* and the ISP subunit in *yellow*. The heme groups of the cyt *b* subunit are shown in stick models with carbon atoms in *yellow*, oxygen in *red*, and nitrogen in *deep blue*. The iron-sulfur cluster (*FeS*) of ISP is shown as the ball and stick model with sulfur in *yellow* and iron in *orange*. Residues from the cyt *b* subunit engaging in interactions with bound inhibitors are labeled and shown as stick models with carbon in *light green*. The two histidine ligands for the iron-sulfur cluster of ISP are also shown as stick models with carbon in *yellow*. Bound inhibitors are shown in stick models with carbon in *black*. They are caged with difference electron density in *blue* calculated with Fourier coefficients $F_o - F_c$ and contoured at 3$\sigma$ levels. The closest distances between one of the histidine ligands of FeS and the bound inhibitors are shown as *dotted lines*. Conserved H-bonds between inhibitors and ligands are given as *dotted lines*.

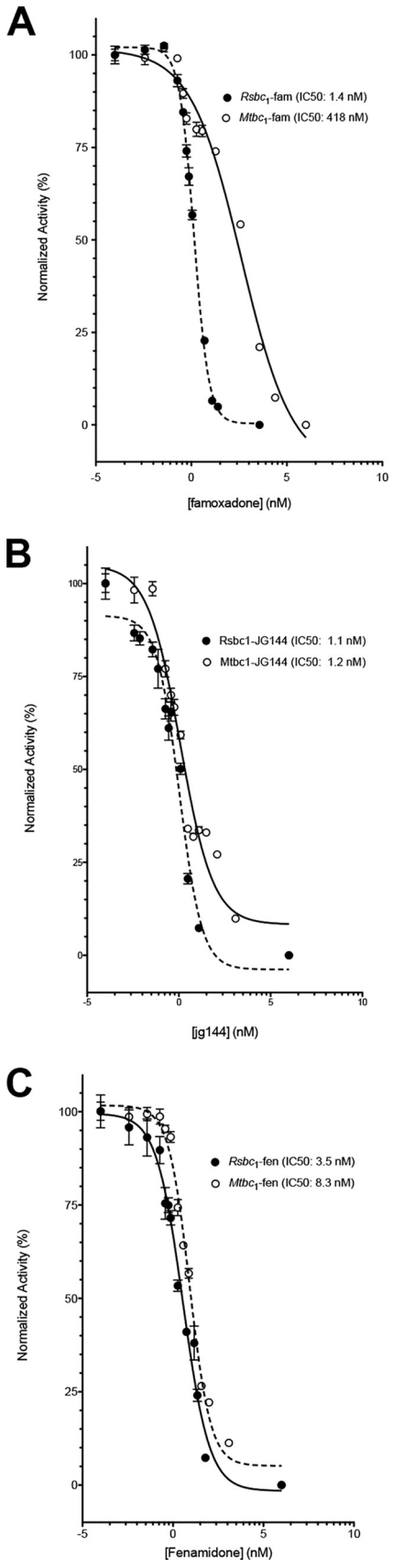


FIGURE 4. **Dose-dependent inhibition of mitochondrial and bacterial cyt $bc_1$ complexes by oxazolidinedinone-type fungicides.** *A*, famoxadone. *B*, jg144. *C*, fenamidone. The activities were normalized to those of uninhibited respective enzymes of $Btbc_1$ and $Rsbc_1$.

characteristic trait of $P_f$-type inhibitors (13), and here the observed shortest distances between $His^{141}$ of the ISP and the bound inhibitors are 6.34 and 6.74 Å, respectively, for jg144 and fenamidone (Fig. 3, *C* and *D*, Table 2). Thus, no direct H-bond is formed between the ISP and the inhibitors.

The structures of both $Btbc_1$·jg144 and $Btbc_1$·fenamidone showed no significant differences in side chain rotamers from $Btbc_1$·famoxadone (Fig. 6*B*). This in turn suggests that the terminal phenoxy group of famoxadone is capable of sampling the environment around the entrance of the $Q_P$ site without perturbing any side chains in the $Q_P$ site. The consistency of interactions and the measurements showing little difference in $IC_{50}$ values between $Btbc_1$ and $Rsbc_1$ for jg144 and fenamidone firmly establish the structural basis for the three-ring unit as the toxophore of the oxazolidinone-type inhibitors (29).

## Discussion

*Mechanistic Implications Concerning the Bifurcated Electron Transfer at the $Q_P$ Site*—Quinol oxidation at the $Q_P$ site requires strict, consecutive bifurcated ET steps that are subject to a high degree of control, an idea that has received support over the years by a substantial amount of experimental evidence and features a bimodal ISP-ED conformation switch at its core (14, 15). Although most structural data on this switch were first obtained from $Btbc_1$, structural information of several avian mitochondrial cyt $bc_1$ ($Ggbc_1$) complexes recently made public in the Protein Data Bank (PDB codes 3L74 and 3L73) is in perfect agreement with the former. However, the conformational switch of the ISP-ED in bacterial $bc_1$ has been difficult to observe crystallographically. This is because all structures of bacterial cyt $bc_1$ complexes obtained so far were crystallized with bound stigmatellin, and it has been difficult to crystallize them in a different $P_f$-type inhibitor such as famoxadone. Conceivably, crystallizing bacterial cyt $bc_1$ bound with a $P_m$-type inhibitor would be even more difficult. Prior to this work, complexes of bacterial $bc_1$ were crystallized only in the presence of the $P_f$–type inhibitor stigmatellin with the ISP-ED immobilized at the $Q_P$ position (4, 12, 17). In this work, we show for the first time that another $P_f$-type inhibitor, namely famoxadone, is able to fix the conformation of ISP-ED without providing a direct H-bond to the ISP subunit, which allows successful crystallization of $Rsbc_1$.

Quinol oxidation at the $Q_P$ site is initiated with the recruitment to and/or stabilization and proper alignment of the ISP-ED at the $Q_P$ site, which was proposed to take place via a direct H-bond between one of the histidine ligands to the 2Fe-2S cluster of ISP ($His^{141}$ in $Btbc_1$ and $His^{152}$ in $Rsbc_1$) and the hydroxyl group of its substrate ubiquinol. This proposal was based on the observation that in high resolution crystal structures, polar atoms from the enzyme's ISP-ED and the inhibitor (specifically stigmatellin and 5-n-heptyl-6-hydroxy-4,7-dioxobenzothiazole (11, 19)) appeared within H-bond distance. Contrary to this view, structural studies with $Btbc_1$ demonstrated that famoxadone is capable of immobilizing the ISP-ED at the $Q_P$ site in the absence of a direct H-bond to the ISP (13, 21). The question becomes whether the presence or absence of the H-bond can support the required bimodal conformation switch of the ISP-ED.

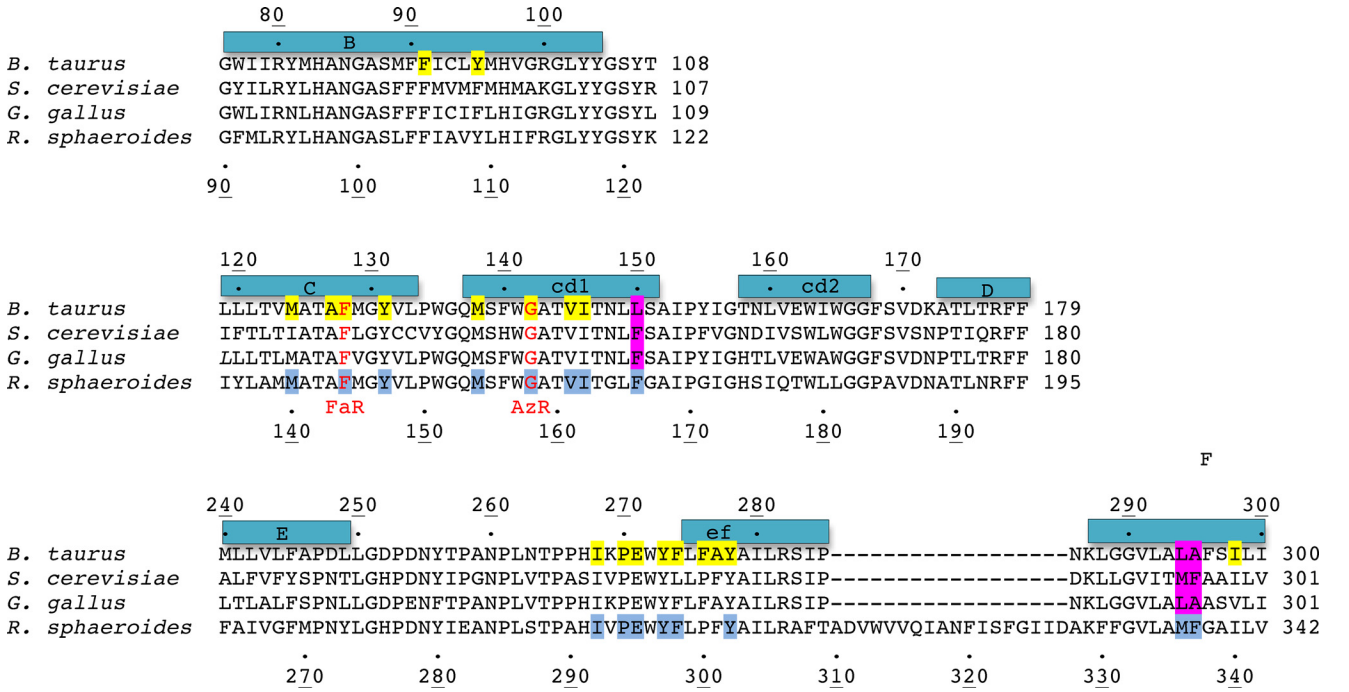


FIGURE 5. **Structure-based sequence alignment of cyt *b* subunits from various organisms.** Only the residues lining the $Q_P$ pocket are shown. *Blue rectangles* placed above sequences are part of helices and are labeled accordingly. Residues whose mutations are known to confer fungicide resistance are in *red*, and the fungicides they are resistant to are indicated below the alignment. *FaR* is short for famoxadone resistance, and *AzR* is for azoxystrobin resistance. Residues that are in direct contact with famoxadone in $Btbc_1$ are highlighted *yellow*. Famoxadone-contacting residues in the $Rsbc_1$ are shaded in *blue*. Differences important for famoxadone binding in avian $bc_1$ are highlighted in *magenta*.

**TABLE 1**

**Statistics on the quality of diffraction data sets of cyt $bc_1$ crystals and structural models**

fen, fenamidone; fam, famoxadone; stg, stigmatellin; ant, antimycin.

| | $Mtbc_1$·fen | $Rsbc_1$·fam | $Rsbc_1$·stg/ant |
|---|---|---|---|
| **Diffraction data** | | | |
| Space group | $I4_122$ | $P1$ | $P1$ |
| Cell parameters | | | |
| $a, b, c$ (Å) | 154.0, 154.0, 592.7 | 120.8, 128.3, 128.3 | 118.9, 126.9, 127.9 |
| $\alpha, \beta, \gamma$ (°) | 90, 90, 90 | 63.9, 88.6, 63.4 | 64.7, 87.7, 61.8 |
| Resolution (Å) (outer shell)[a] | 50–2.5 (2.59–2.50) | 31.9–2.95 (3.06–2.95) | 37.8–3.00 (3.10–3.00) |
| $R_{merge}$ | 0.091 (0.442) | 0.102 (0.549) | 0.175 (0.730) |
| Completeness (%) | 98.5 (97.8) | 96.5 (89.1) | 93.6 (81.1) |
| $<I>/\sigma_I$ | 13.8 (2.0) | 5.6 (1.2) | 5.0 (1.4) |
| No. unique obs. | 120,848 (11,829) | 122,242 (11,289) | 110,064 (9,558) |
| **Refinement** | | | |
| Resolution (Å)[a] | 34.3–2.65 (2.75–2.65) | 29.7–2.97 (3.04–2.97) | 37.7–3.00 (3.07–3.00) |
| $R_{free}$ | 0.269 (0.343) | 0.258 (0.337) | 0.243 (0.374) |
| $R_{work}$ | 0.228 (0.338) | 0.215 (0.362) | 0.211 (0.329) |
| No. atoms | 16,913 | 27,918 | 27,938 |
| No. residues | 2,079 | 3,484 | 3,476 |
| No. ligand atoms | 548 | 962 | 1022 |
| No. solvent molecules | 50 | 4 | 0 |
| RMS deviations | | | |
| Bond length | 0.005 | 0.014 | 0.01 |
| Bond angles | 0.75 | 1.33 | 1.13 |
| Ramachandran plot | | | |
| Favored (%) | 96 | 97 | 95 |
| Outliers (%) | 0.34 | 0.2 | 0.12 |

[a] The statistics for the highest resolution shell are shown in parentheses.

The bifurcated ET at the $Q_P$ site begins with the binding of substrate $QH_2$, which also triggers the docking of ISP-ED. An H-bond forms between a hydroxyl group of $QH_2$ and a histidine of the ISP-ED. After deprotonation, the $QH_2$ transfers its first electron to the 2Fe-2S cluster of the ISP, which is an energetically favorable process. The second electron of $QH_2$, however, has to travel to the $Q_N$ site via the hemes, $b_L$ and $b_H$, eventually reducing a ubiquinone (Q) or ubisemiquinone ($Q^{\bullet}$) molecule (Fig. 1*B*). It is important to emphasize (i) that to avoid short circuit reactions, the 2Fe-2S cluster cannot be allowed to leave the $Q_P$ site and return oxidized until the product has been completely removed and/or replaced by $QH_2$ and (ii) that although the ISP-ED remains at the $Q_P$ site, the H-bond should always exist between the reduced ISP and the product ubiquinone (Q) after the completion of the two-electron transfer reaction (Fig. 7). In other words, the H-bond between the substrate and the ISP cannot control the conformation switch of the ISP-ED.

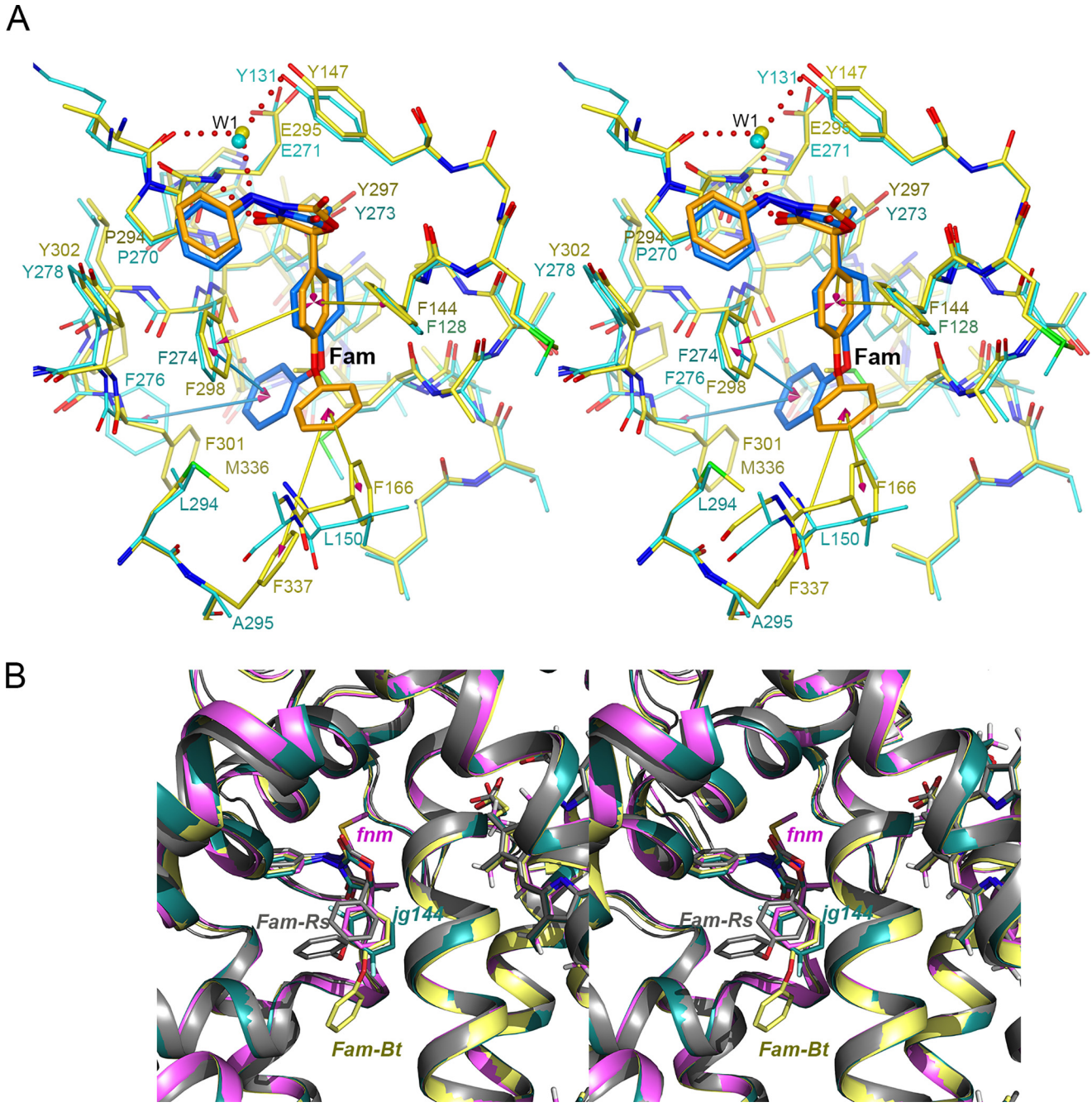


FIGURE 6. **Species-dependent inhibitor binding.** *A*, stereoscopic pairs showing differences in the $Q_P$ environment between *Btbc*$_1$ and *Rsbc*$_1$ upon famoxadone binding. Cyt *b* subunits of *Btbc*$_1$·famoxadone and *Rsbc*$_1$·famoxadone structures were superposed. Residues surrounding the $Q_P$ pocket are shown in stick models with carbon atoms in *yellow* for *Rsbc*$_1$ and in *cyan* for *Btbc*$_1$. Oxygen and nitrogen atoms are shown in *red* and *blue*, respectively. Key residues for binding are labeled with *Rsbc*$_1$ in *yellow* and *Btbc*$_1$ in *cyan*. The bound famoxadones are shown in *coral* and *blue* for *Rsbc*$_1$ and *Btbc*$_1$, respectively. Torsion angles around the four atoms C12-C11-O14-C15 are −116° for *Btbc*$_1$·famoxadone and +145° for *Rsbc*$_1$·famoxadone. *B*, stereodiagram showing conformations of bound oxazolidinedion-type inhibitors based on superposition of structures of mitochondrial cyt *b* with bound famoxadone (*yellow*), jg144 (*cyan*), and fenamidone (*magenta*) and of the structure of *Rsbc*$_1$ with bound famoxadone (*gray*).

In this work, we present evidence from the famoxadone-bound *Rsbc*$_1$ structure and two *Btbc*$_1$ structures with bound oxazolidinedione-type inhibitors, jg144 and fenamidone, showing that docking of the ISP-ED to the $Q_P$ site, both in mitochondrial and bacterial cyt $bc_1$, does not require a direct H-bond between the ISP and the inhibitor. This lends strong support for the hypothesis that electron bifurcation at the $Q_P$ site is achieved through a controlled bimodal conformational change of the ISP-ED (14, 15).

*Crystal Contacts Do Not Significantly Influence the Conformation of ISP-ED*—The head domain of ISP in *Rsbc*$_1$ is involved in crystal-packing contacts, whereas that of *Btbc*$_1$ is not. This observation provides a good opportunity to qualitatively assess how much influence crystal contacts have on the conformation of the intrinsically moving domain. For the purpose of an unbiased comparison, we also determined the structure of the doubly inhibited (stigmatellin and antimycin) ternary complex of *Rsbc*$_1$ (Table 1). Antimycin is a $Q_N$ site inhibitor and is not

known to influence ISP-ED conformation; thus, its presence is of no consequence for this analysis. Stigmatellin inhibited $Rsbc_1$ has been structurally characterized before (4). However, the newly determined structure that we are using as a reference was obtained from the same batch of protein under the same conditions, and importantly, the crystals features the same space group *P*1, the same number of molecules per asymmetric unit (two dimers) and has the same cell dimensions and crystal packing. To quantify how much the ISP-ED moves in response to a change in the $Q_P$ site occupant, we superposed only the C$\alpha$ atoms of the cyt *b* subunits of the different complexes (stigmatellin *versus* famoxadone) and calculated the respective RMS deviations of the head domain of the ISP, cyt *b*, and cyt $c_1$ subunits (Table 3). Although the C$\alpha$ traces of cyt *b* superimpose very well (<0.4 Å), the traces of the ISP-ED no longer coincide: they display RMS deviations as large as 2.55 Å (139 C$\alpha$) and 2.86 Å (124 C$\alpha$), respectively, for $Rsbc_1$ and $Btbc_1$. This is significant, because the corresponding deviations of the head domain of cyt $c_1$ (a domain that is spatially close to ISP-ED and located in the same aqueous phase) amounted to an RMS deviation of only 0.60 Å ($Rsbc_1$) and 0.93 Å ($Btbc_1$), respectively. It is worth noting that the RMS deviations of ISP-ED in $Rsbc_1$ and $Btbc_1$ are nearly the same despite the fact that the ISP-ED of the $Rsbc_1$ is clearly involved in crystal contacts, unlike the ISP-ED in $Btbc_1$, which has none. The similarities in RMS deviations between $Rsbc_1$ and $Btbc_1$ suggest that the crystal contacts in $Rsbc_1$ play only a secondary role in determining the final conformation of the ISP-ED once ISP-ED is docked at the $Q_P$ site.

The angular displacement of the ISP-EDs between $Btbc_1$ and $Rsbc_1$ when bound with different inhibitors can also be visualized using vectors (Fig. 8*A*), which is calculated based on superposition of cyt *b* subunits only between the structures with bound antimycin and famoxadone. The *red vectors* in the ISP trace (*yellow trace*) of the stigmatellin-inhibited $Rsbc_1$ represent the connection to the C$\alpha$ atoms of the famoxadone-inhibited complex. The *blue vectors* represent the equivalent repositioning of the C$\alpha$ atoms of the ISP-ED in $Btbc_1$. This vector diagram illustrates qualitatively that the amount of change (vector length) is approximately the same in both sets. However, the direction in which the ISP-ED is displaced in $Rsbc_1$,

**TABLE 2**

**Normalized anomalous peak heights for iron atoms in crystals of bovine mitochondrial $bc_1$ in complex with oxazolidinedione inhibitors**

| Bound inhibitor | cyt $bc_1$ complex | Distance to ISP | Normalized anomalous peak height[a] | | | | Inhibitor class |
|---|---|---|---|---|---|---|---|
| | | | $b_H$ | $b_L$ | $c_1$ | ISP | |
| | | Å | | | | | |
| Stigmatellin[b,c] | $Btbc_1$ | 3.03 | 1.0 | 0.99 | 0.81 | 1.20 | $P_f$ |
| Famoxadone | $Btbc_1$ | 6.07 | 1.0 | 0.85 | 0.64 | 1.02 | $P_f$ |
| Fenamidone | $Btbc_1$ | 6.74 | 1.0 | 0.80 | 0.67 | 0.94 | $P_f$ |
| JG144 | $Btbc_1$ | 6.34 | 1.0 | 0.91 | 0.78 | 1.30 | $P_f$ |
| Azoxystrobin[c] | $Btbc_1$ | | 1.0 | 0.85 | 0.95 | 0.36 | $P_m$ |
| Stigmatellin[d] | $Rsbc_1$ | 2.84 | 1.0 | | | | $P_f$ |
| Famoxadone[d] | $Rsbc_1$ | 5.73 | 1.0 | | | | $P_f$ |

[a] The peaks are normalized against anomalous signals of their respective $b_H$ heme irons.
[b] Anomalous signals were calculated using diffraction data in the range of 20–5 Å.
[c] These numbers were taken from Esser *et al.* (13) for comparison.
[d] These two inhibitors fix ISP-ED to the *b* site allowing $Rsbc_1$ to be crystallized. However, because of crystal contact, the anomalous peak heights are not considered reflecting a true state of equilibration in solution.

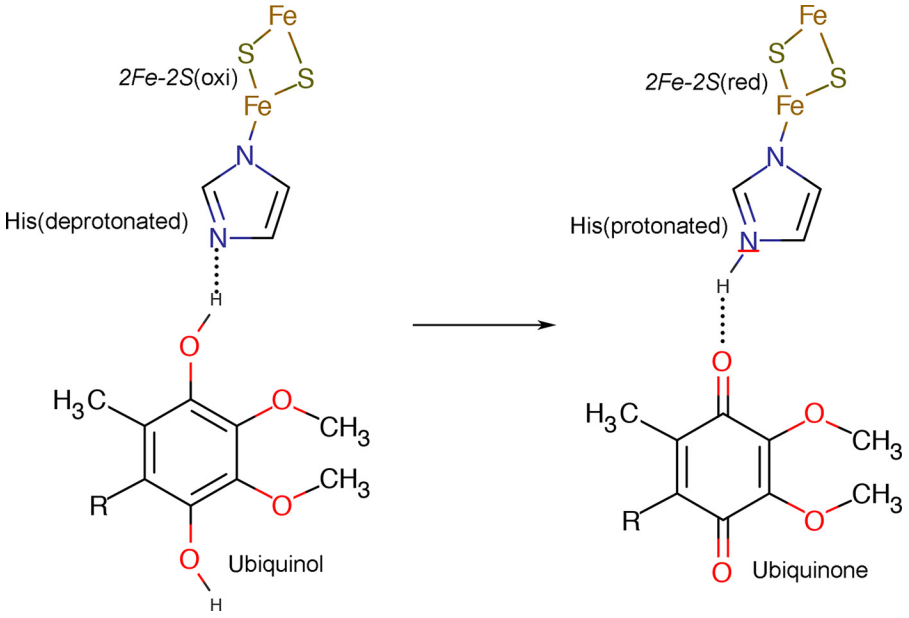


FIGURE 7. **H-bond between substrate and histidine ligand of 2Fe-2S cluster before and after ET reaction at the $Q_P$ site.**

**TABLE 3**

**RMS deviation values of C$\alpha$ traces between equivalent subunits in stigmatellin *versus* famoxadone inhibited cyt $bc_1$ after superimposing cyt *b* subunit only**

| Structures | RMS deviation of stigmatellin *vs.* famoxadone | | |
|---|---|---|---|
| | cyt *b* | ISP-ED | cyt $c_1$ |
| | | Å | |
| $Rsbc_1$ (residue range, no. residue) | 0.40 (3–430, 428) | 2.55 (49–187, 139) | 0.60 (1–222, 222) |
| $Btbc_1$ (residue range, no. residue) | 0.40 (10–378, 369) | 2.86 (73–196, 124) | 0.93 (1–197, 197) |

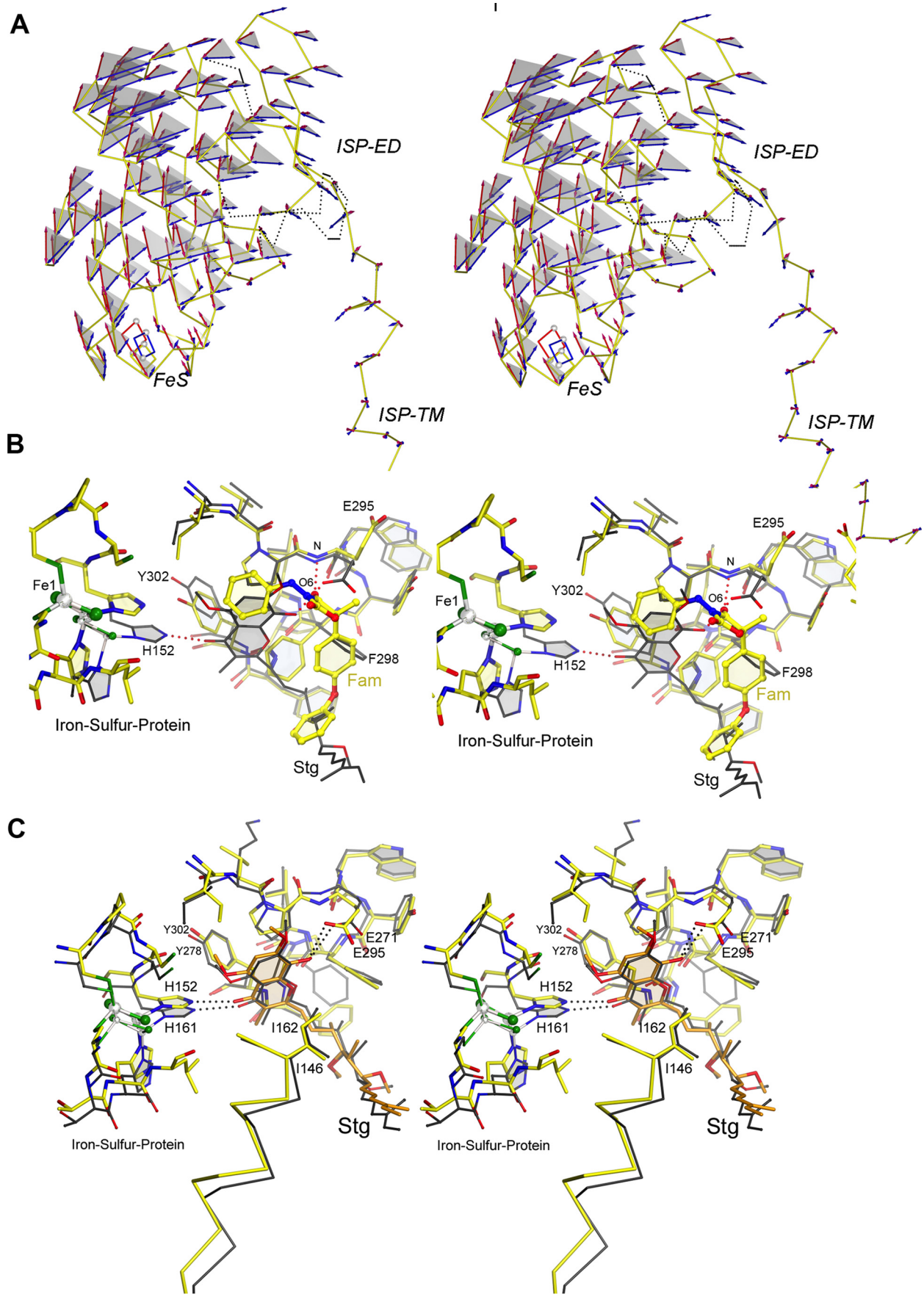
A
ISP-ED
FeS
ISP-TM
ISP-ED
FeS
ISP-TM
B
E295
N
Y302
O6
Fe1
H152
F298
Fam
Iron-Sulfur-Protein
Stg
E295
N
Y302
O6
Fe1
H152
F298
Fam
Iron-Sulfur-Protein
Stg
C
Y302
Y278
E271
E295
H152
H161
I162
I146
Stg
Iron-Sulfur-Protein
Y302
Y278
E271
E295
H152
H161
I162
I146
Stg
Iron-Sulfur-Protein

*versus* $Btbc_1$, is characterized by an angle of 58° (represented by half-transparent triangles). It is conceivable that, as a consequence of packing forces in $Rsbc_1$ crystals, the ISP-ED undergoes an angular adjustment but importantly maintains the proper distance from the $Q_P$ site of cyt *b*.

*Implications Concerning the Design and Use of Broad Spectrum Antifungal Agents*—Despite considerable pressure that must exist to maintain the intricate function of cyt *b* and its active sites, several residues, individually or in groups, may have changed in the course of evolution. These changes are seen as the root cause of intrinsic drug resistance by target site mutations. By determining the structure of $Rsbc_1$ in complex with famoxadone and comparing it with that of $Btbc_1$, we uncovered the structural basis for the effects of sequence polymorphisms on the binding of inhibitors to cyt $bc_1$ of different organisms, which were manifested by varied efficacies of inhibitors against cyt $bc_1$ complexes. This structural observation is consistent with measurements of $IC_{50}$ values, indicating that famoxadone inhibits $Rsbc_1$ more strongly than $Btbc_1$ (Fig. 4*A*); it agrees also with the binding energy of −12.0 kcal/mol and −12.8 kcal/mol, respectively, estimated by molecular docking experiments for mitochondrial and bacterial cyt $bc_1$ complexes. The conformation of famoxadone in the binding pocket shows sensitivity to the environment and is characterized by a tendency to optimize Ar-Ar interactions (21).

Because of the absence of an apo $Rsbc_1$ structure, the only comparisons that can be made are between complexes of $Rsbc_1$ with famoxadone and stigmatellin (Fig. 8*B*) and the equivalent pair of $Btbc_1$ complexes (Fig. 8*C*). The comparison made it immediately clear that the accommodation of famoxadone in the $Q_P$ pocket requires adjustments of torsion angles in both the inhibitors and cyt *b* residues. Direct steric interactions force $Phe^{298}$ ($Phe^{274}$ in $Btbc_1$) to adopt two distinct conformations depending on the binding of either stigmatellin or famoxadone in both $Rsbc_1$ and $Btbc_1$. Similarly pronounced are changes in the positions of $Glu^{295}$ ($Glu^{271}$ in $Btbc_1$) in response to the inhibitors. In the $Rsbc_1$·famoxadone structure, $Glu^{295}$ returns to the solvent channel or to the "native" position as observed in $Btbc_1$ structures because of the loss of a hydrogen bond to the inhibitor (8).

From the $Rsbc_1$ structure, $Phe^{166}$, $Met^{336}$, and $Phe^{337}$ ($Leu^{150}$, $Leu^{294}$, and $Ala^{295}$ in $Btbc_1$) appear to play a major role in repositioning the terminal phenoxy moiety of famoxadone. Although this is convincing based on qualitative energy considerations, the situation seems subtler in the recently published $Ggbc_1$ structure with famoxadone (35), showing the same moiety in an orientation nearly identical to the one found in $Rsbc_1$ but in contrast to that in $Btbc_1$. Despite the higher sequence identity between $Ggbc_1$ and $Btbc_1$ (Fig. 5), residue $Phe^{151}$ in the avian *Gg* cyt *b* is also a phenylalanine, as in $Rsbc_1$ ($Rsbc_1$ $Phe^{166}$). However, residue $Phe^{337}$ of *Rs* cyt *b* coincides with the non-aromatic $Ala^{296}$ in *Gg* cyt *b*, implying that a single change in the amino acid composition ($Leu^{150}Phe$) at the entrance to the $Q_P$ pocket is sufficient to stabilize an alternate conformation of famoxadone to the one that was first found in $Btbc_1$. This observation underscores the importance of Ar-Ar interaction in inhibitor binding.

The fact that famoxadone is able to adapt to the different microenvironments of the target sites of a wide range of organisms suggests two important principles for designs of broad spectrum inhibitors: one is the flexibility to adopt different conformations as needed, and the other is the ability to fully engage in Ar-Ar interactions. A single pair of Ar-Ar interactions could provide as much as 1.3 kcal/mol of free energy (36), which can be exploited either for the enhancement of specificity or for the evasion of resistance and is also consistent with previous observations that the phenoxyphenyl group of famoxadone is most tolerant to variations (29).

## Experimental Procedures

*Expression of Δ-sub IV $Rsbc_1$*—The purification procedure for $Rsbc_1$, published earlier (37), was used with minor changes to obtain protein for crystallization. Briefly, chromatophore membranes were prepared from cells harboring the plasmid (pRKD*fbcFBC*$_H$) coding for Δ-sub IV wild type $Rsbc_1$ protein, by disrupting cells with a French press followed by differential centrifugations. To purify $His_6$-tagged $Rsbc_1$, the chromatophore suspensions were adjusted to a cyt *b* concentration of 25 μM with 50 mM Tris-Cl (pH 8.0 at 4 °C), containing 20% glycerol, 1 mM $MgSO_4$, and 1 mM PMSF. Dodecyl-D-maltopyranoside (DDM) solution (10% w/v) was added dropwise to a final detergent to protein ratio of 0.57 (mg/mg). After centrifugation, the supernatant was loaded on a nickel-nitrilotriacetic acid column, which was washed with 6 column volumes of buffer A (50 mM Tris-HCl, pH 8.0, at 4 °C, 200 mM NaCl, 0.01% DDM), 6 column volumes of buffer A in the presence of 5 mM histidine, and 4 column volumes of buffer B (50 mM Tris-HCl, pH 8.0, at 4 °C, 200 mM NaCl, 0.5% β-OG) in the presence of 5 mM histidine. The desired protein fractions were eluted with buffer B containing 200 mM histidine and concentrated with Centriprep-50 to a final concentration of 300 μM.

*Crystallization of $Btbc_1$ in Complex with Inhibitors*—The final concentration of purified $Btbc_1$ complex was adjusted to 20 mg/ml in a solution containing 50 mM MOPS buffer at pH 7.2, 20 mM ammonium acetate, 20% (w/v) glycerol, and 0.16% sucrose monocaprate. This solution was further incubated with a 5× molar excess amount of the desired inhibitor and set up for crystallization as described in previous publications (8, 21). Crystals were treated with a cryoprotectant in 5% increments until the final glycerol concentration reached 42% and then cryo-cooled in liquid propane.

FIGURE 8. **Stereoscopic pairs showing the changes in subunits of cyt $bc_1$ upon binding of different inhibitors.** *A*, effects of inhibitor binding on the conformation of ISP-ED. The tracing of the Cα atoms of the ISP-ED from $Rsbc_1$ in complex with stigmatellin is drawn in *yellow*. A *red vector* marks the distance to the same Cα atom of $Rsbc_1$ in complex with famoxadone. The *blue vectors* represent changes in Cα positions between famoxadone- and stigmatellin-bound $Btbc_1$. The *dotted lines* connect residues that have no equivalent in $Btbc_1$. *B*, superposition of the cyt *b* subunits of $Rsbc_1$·famoxadone and $Rsbc_1$·stigmatellin. The famoxadone bound structure is shown with carbon atoms in *yellow*, whereas that with bound stigmatellin is given with carbon atoms in *gray*. In both structures, nitrogen atoms are colored *blue*, and oxygen is *red*. Residues that undergo large conformational changes with different inhibitors bound are labeled. *C*, superposition of the cyt *b* subunits of $Btbc_1$·famoxadone and $Btbc_1$·stigmatellin.

*Crystallization of Famoxadone-inhibited $Rsbc_1$*—A solution of Δ-sub IV $Rsbc_1$ (57 mg/ml) in a buffer containing 0.5% β-OG was treated overnight with a 3-fold molar excess of famoxadone (Chem. Service Inc.). The solution was diluted 4-fold with buffer consisting of 50 mM Tris-HCl, pH 8.0, 0.3% β-OG, 200 mM histidine, 150 mM NaCl, 10 mM sodium ascorbate, and 10% glycerol. The resulting solution of 14 mg/ml $Rsbc_1$ in 0.35% β-OG was augmented with sucrose monocaprate (0.06%, ~0.5 critical micelle concentration) and 10 mM strontium nitrate. PEG 400, added to a final concentration of 7%, served as the precipitant. The solution was allowed to stand overnight at 4 °C. Any precipitate was centrifuged off, and 5 μl of the supernatant was used in sitting drop vapor diffusion crystallization trays over 1 ml of 100 mM Tris-HCl, pH 8.0, 20% glycerol, 600 mM NaCl, 26% PEG 400, and 5 mM $NaN_3$. After several weeks, small red crystals appeared which froze cleanly in liquid propane without requiring additional cryoprotectants.

*Diffraction Data Collection, Structure Determination, and Refinement*—Crystals of the tetragonal $Btbc_1$·fenamidone and the triclinic famoxadone-inhibited $Rsbc_1$ were stable when cryo-cooled to 100 K, permitting several hours of data collection at the SER-CAT Beamline (ID22) of the Advanced Photon Source, Argonne National Lab. Raw diffraction frames were processed with the program package HKL2000 (38). A diffraction data set for the $Btbc_1$ crystal was phased with coordinates of the 11-subunit apo structure of $Btbc_1$ (PDB code 1NTM) (23). The program REFMAC (39) was employed for initial rigid body refinement followed by iterative maximum likelihood and TLS (Translation, Libration, and Screw tensor) refinement. In between REFMAC runs, sigma A (40) weighted $2F_o - F_c$ and $F_o - F_c$ Fourier maps were calculated and used to identify and build bound ligand and solvent molecules manually with the program Coot (41). The data set for the $Rsbc_1$ was phased with molecular replacement using an edited version of the $Rsbc_1$ dimer (PDB code 2QJY) in MolRep (CCP4) (42), producing a solution with two dimers/unit cell. Care was taken in the subsequent refinement to allow the head domain of the ISP to adjust to a position possibly different from that in stigmatellin-inhibited complexes. Rigid body refinement, simulated annealing, positional, and atomic displacement (ADP, TLS) refinement were carried out with phenix.refine 1.8–1512 (43). 4-fold NCS restraints were applied throughout the refinement. However, no NCS restraints were imposed on the four famoxadone molecules during refinement, yet they are superposed within 0.2 Å RMS deviation (average from mean structure), allowing our analysis to focus on just one molecule. Manual adjustments of the coordinates were carried out in O (44) and Coot 0.6. As the last step, famoxadone was fitted into the difference density. Final refinement statistics are given in Table 2.

*Measurement of $IC_{50}$ Values for $bc_1$ Inhibitors*—The activities of $Mtbc_1$ and $Rsbc_1$ were assayed following the reduction of substrate cyt *c*. The $bc_1$ preparation was diluted to a final concentration of 0.1 and 1 μM, respectively, for $Btbc_1$ and $Rsbc_1$ in a buffer containing 50 mM Tris-HCl, pH 8.0, 0.01% β-DDM, and 200 mM NaCl. To a 2-ml assay mixture containing 100 mM phosphate buffer, pH 7.4, 0.3 mM EDTA, and 80 μM cyt *c*, $Q_0C_{10}BrH_2$ was added to a final concentration of 25 μM, and the solution was split evenly into two cuvettes. To one cuvette, 5 μl of diluted $bc_1$ solution was added, and we immediately began recording the cyt *c* reduction at 550-nm wavelengths for 100 s in a two-beam Shimadzu UV-2250 PC spectrophotometer at room temperature. The amount of cyt *c* reduced at a given period of time was calculated using a millimolar extinction coefficient of 18.5 $mM^{-1}$ $cm^{-1}$. To measure the effect of $bc_1$ inhibitors, $bc_1$ was preincubated with various concentrations of inhibitors for 5 min on ice prior to the measurement of $bc_1$ activity. The $IC_{50}$ value for each inhibitor was calculated by a least squares procedure fitting the equation ($Y = A_{min} + (A_{max} - A_{min})/(1 + 10^{(X\text{-}logIC_{50})})$) implemented in a commercial package Prism, where $A_{max}$ and $A_{min}$ are maximal and minimal activities, respectively.

*Author Contributions*—D. X. conceived and coordinated this study and wrote most of this paper. L. E. wrote significant parts of this paper, prepared Figs. 1 and 8, and crystallized and solved the structures of RS·fam and RS·stg/an. F. Z. expressed and purified *R. sphaeroides* $bc_1$ needed in this study and performed the assays in Fig. 4. Y. Z., Y. X., and Z. Q. contributed to the crystallization and structure determination of $Btbc_1$·fenamidone complex. W.-K. T. advised on the interpretation of the kinetics of the binding studies. C.-A. Y. contributed to the discussion and interpretation of the effect of inhibitors in $bc_1$.

*Acknowledgments—We thank the staff of SER-CAT at Advanced Photon Source, Argonne National Lab for assistance in data collection and George Leiman for helping with manuscript preparation. The compound jg144 was a gift from Dr. Steve. O. Pember (Dupont). This study utilized the high-performance computational capabilities of the Biowulf Linux cluster at the National Institutes of Health.*

**References**

1. Trumpower, B. L. (1990) Cytochrome $bc_1$ complexes of microorganisms. *Microbiol. Rev.* **54,** 101–129
2. Keilin, D. (1925) On cytochrome, a respiratory pigment, common to animals, yeast, and higher plants. *Proc. R. Soc. Lond. B* **98,** 312–399
3. Ljungdahl, P. O., Pennoyer, J. D., Robertson, D. E., and Trumpower, B. L. (1987) Purification of highly active cytochrome bc1 complexes from phylogenetically diverse species by a single chromatophaphic procedure. *Biochim. Biophys. Acta* **891,** 227–241
4. Esser, L., Elberry, M., Zhou, F., Yu, C. A., Yu, L., and Xia, D. (2008) Inhibitor complexed structures of the cytochrome $bc_1$ from the photosynthetic bacterium *Rhodobacter sphaeroides* at 2.40 Å resolution. *J. Biol. Chem.* **283,** 2846–2857
5. Mitchell, P. (1975) Protonmotive redox mechanism of the cytochrome $bc_1$ complex in the respiratory chain: protonmotive uniquinone cycle. *FEBS Lett.* **56,** 1–6
6. Crofts, A. R., Meinhardt, S. W., Jones, K. R., and Snozzi, M. (1983) The role of the quinone pool in the cyclic electron-transfer chain of *Rhodopseudomonas sphaeroides*: a modified q-cycle mechanism. *Biochim. Biophys. Acta* **723,** 202–218
7. Trumpower, B. L. (1990) The protonmotive Q cycle. Energy transduction by coupling of proton translocation to electron transfer by the cytochrome $bc_1$ complex. *J. Biol. Chem.* **265,** 11409–11412
8. Xia, D., Yu, C. A., Kim, H., Xia, J. Z., Kachurin, A. M., Zhang, L., Yu, L., and Deisenhofer, J. (1997) Crystal structure of the cytochrome $bc_1$ complex from bovine heart mitochondria. *Science* **277,** 60–66
9. Iwata, S., Lee, J. W., Okada, K., Lee, J. K., Iwata, M., Rasmussen, B., Link, T. A., Ramaswamy, S., and Jap, B. K. (1998) Complete structure of the 11-subunit bovine mitochondrial cytochrome $bc_1$ complex [see comments]. *Science* **281,** 64–71

10. Zhang, Z., Huang, L., Shulmeister, V. M., Chi, Y. I., Kim, K. K., Hung, L. W., Crofts, A. R., Berry, E. A., and Kim, S. H. (1998) Electron transfer by domain movement in cytochrome $bc_1$. *Nature* **392,** 677–684
11. Hunte, C., Koepke, J., Lange, C., Rossmanith, T., and Michel, H. (2000) Structure at 2.3 A resolution of the cytochrome $bc_1$ complex from the yeast *Saccharomyces cerevisiae* co-crystallized with an antibody Fv fragment. *Structure* **8,** 669–684
12. Kleinschroth, T., Castellani, M., Trinh, C. H., Morgner, N., Brutschy, B., Ludwig, B., and Hunte, C. (2011) X-ray structure of the dimeric cytochrome $bc_1$ complex from the soil bacterium *Paracoccus denitrificans* at 2.7-Å resolution. *Biochim. Biophys. Acta* **1807,** 1606–1615
13. Esser, L., Quinn, B., Li, Y. F., Zhang, M., Elberry, M., Yu, L., Yu, C. A., and Xia, D. (2004) Crystallographic studies of quinol oxidation site inhibitors: a modified classification of inhibitors for the cytochrome $bc_1$ complex. *J. Mol. Biol.* **341,** 281–302
14. Esser, L., Gong, X., Yang, S., Yu, L., Yu, C. A., and Xia, D. (2006) Surface-modulated motion switch: capture and release of iron-sulfur protein in the cytochrome $bc_1$ complex. *Proc. Natl. Acad. Sci. U.S.A.* **103,** 13045–13050
15. Xia, D., Esser, L., Tang, W. K., Zhou, F., Zhou, Y., Yu, L., and Yu, C. A. (2013) Structural analysis of cytochrome $bc_1$ complexes: implications to the mechanism of function. *Biochim. Biophys. Acta* **1827,** 1278–1294
16. Huang, L. S., Cobessi, D., Tung, E. Y., and Berry, E. A. (2005) Binding of the respiratory chain inhibitor antimycin to the mitochondrial $bc_1$ complex: a new crystal structure reveals an altered intramolecular hydrogen-bonding pattern. *J. Mol. Biol.* **351,** 573–597
17. Berry, E. A., Huang, L. S., Saechao, L. K., Pon, N. G., Valkova-Valchanova, M., and Daldal, F. (2004) X-ray structure of *Rhodobacter capsulatus* cytochrome $bc_1$: comparison with its mitochondrial and chloroplast counterparts. *Photosynth. Res.* **81,** 251–275
18. Palsdottir, H., Lojero, C. G., Trumpower, B. L., and Hunte, C. (2003) Structure of the yeast cytochrome $bc_1$ complex with a hydroxyquinone anion Qo site inhibitor bound. *J. Biol. Chem.* **278,** 31303–31311
19. Berry, E. A., and Huang, L. (2003) Observations concerning the quinol oxidation site of the cytochrome $bc_1$ complex. *FEBS Lett.* **555,** 13–20
20. Crofts, A. R., Barquera, B., Gennis, R. B., Kuras, R., Guergova-Kuras, M., and Berry, E. A. (1999) Mechanism of ubiquinol oxidation by the $bc_1$ complex: different domains of the quinol binding pocket and their role in the mechanism and binding of inhibitors. *Biochemistry* **38,** 15807–15826
21. Gao, X., Wen, X., Yu, C., Esser, L., Tsao, S., Quinn, B., Zhang, L., Yu, L., and Xia, D. (2002) The crystal structure of mitochondrial cytochrome $bc_1$ in complex with famoxadone: the role of aromatic-aromatic interaction in inhibition. *Biochemistry* **41,** 11692–11702
22. Willis, R. J. (2007) *The History of Allelopathy*, Springer, Dordrecht, The Netherlands
23. Gao, X., Wen, X., Esser, L., Quinn, B., Yu, L., Yu, C. A., and Xia, D. (2003) Structural basis for the quinone reduction in $bc_1$ complex: a comparative analysis of crystal structures of mitochondrial cytochrome $bc_1$ with bound substrate and inhibitors. *Biochemistry* **42,** 9067–9080
24. Brandt, U., and von Jagow, G. (1991) Analysis of inhibitor binding to the mitochondrial cytochrome *c* reductase by fluorescence quench titration. *Eur. J. Biochem.* **195,** 163–170
25. Brandt, U., and Djafarzadeh-Andabili, R. (1997) Binding of MOA-stilbene to the mitochondrial cytochrome $bc_1$ complex is affected by the protonation state of a redox-Bohr group of the Rieske iron-sulfur protein. *Biochim. Biophys. Acta* **1321,** 238–242
26. Ohnishi, T., Brandt, U., and von Jagow, G. (1988) Studies on the effect of stigmatellin derivatives on cytochrome *b* and the Rieske iron-sulfur cluster of cytochrome *c* reductase from bovine heart mitochondria. *Eur. J. Biochem.* **176,** 385–389
27. Link, T. A., Haase, U., Brandt, U., and von Jagow, G. (1993) What information do inhibitors provide about the structure of the hydroquinone oxidation site of ubihydroquinone: cytochrome *c* oxidoreductase? *J. Bioenerg. Biomembr.* **25,** 221–232
28. Brandt, U., Schägger, H., and von Jagow, G. (1988) Characterisation of binding of the methoxyacrylate inhibitors to mitochondrial cytochrome *c* reductase. *Eur. J. Biochem.* **173,** 499–506
29. Sternberg, J. A., Geffken, D., Adams, J. B., Jr., Pöstages, R., Sternberg, C. G., Campbell, C. L., and Moberg, W. K. (2001) Famoxadone: the discovery and optimisation of a new agricultural fungicide. *Pest. Manag. Sci.* **57,** 143–152
30. Jordan, D. B., Livingston, R. S., Bisaha, J. J., Duncan, K. E., Pember, S. O., Picollelli, M. A., Schwartz, R. S., Sternberg, J. A., and Tang, X. S. (1999) Mode of action of famoxadone. *Pest. Sci.* **55,** 105–118
31. Fernández-Ortuño, D., Torés, J. A., de Vicente, A., and Pérez-García, A. (2008) Field resistance to QoI fungicides in *Podosphaera fusca* is not supported by typical mutations in the mitochondrial cytochrome *b* gene. *Pest. Manag. Sci.* **64,** 694–702
32. Steinfeld, U., Sierotzki, H., Parisi, S., Poirey, S., and Gisi, U. (2001) Sensitivity of mitochondrial respiration to different inhibitors in *Venturia inaequalis*. *Pest. Manag. Sci.* **57,** 787–796
33. Genet, J. L., Jaworska, G., and Deparis, F. (2006) Effect of dose rate and mixtures of fungicides on selection for QoI resistance in populations of *Plasmopara viticola*. *Pest. Manag. Sci.* **62,** 188–194
34. Chen, W. J., Delmotte, F., Richard-Cervera, S., Douence, L., Greif, C., and Corio-Costet, M. F. (2007) At least two origins of fungicide resistance in grapevine downy mildew populations. *Appl. Environ. Microbiol.* **73,** 5162–5172
35. Berry, E. A., and Huang, L. S. (2011) Conformationally linked interaction in the cytochrome $bc_1$ complex between inhibitors of the Q(o) site and the Rieske iron-sulfur protein. *Biochim. Biophys. Acta* **1807,** 1349–1363
36. Serrano, L., Bycroft, M., and Fersht, A. R. (1991) Aromatic-aromatic interactions and protein stability: investigation by double-mutant cycles. *J. Mol. Biol.* **218,** 465–475
37. Xiao, Y. M., Esser, L., Zhou, F., Li, C., Zhou, Y. H., Yu, C. A., Qin, Z. H., and Xia, D. (2014) Studies on inhibition of respiratory cytochrome $bc_1$ complex by the fungicide pyrimorph suggest a novel inhibitory mechanism. *PLoS One* **9,** e93765
38. Otwinowski, Z., and Minor, W. (1997) Processing of X-ray diffraction data collected in oscillation mode. *Methods Enzymol.* **276,** 307–326
39. Murshudov, G. N., Vagin, A. A., and Dodson, E. J. (1997) Refinement of macromolecular structures by the maximum-likelihood method. *Acta Crystallogr. D* **53,** 240–255
40. Read, R. J. (1986) Improved Fourier coefficients for maps using phases from partial structures with errors. *Acta Crystallogr. A* **42,** 140–149
41. Emsley, P., and Cowtan, K. (2004) Coot: model-building tools for molecular graphics. *Acta Crystallogr. D Biol. Crystallogr.* **60,** 2126–2132
42. Vagin, A., and Teplyakov, A. (2000) An approach to multi-copy search in molecular replacement. *Acta Crystallogr. D Biol. Crystallogr.* **56,** 1622–1624
43. Adams, P. D., Grosse-Kunstleve, R. W., Hung, L. W., Ioerger, T. R., McCoy, A. J., Moriarty, N. W., Read, R. J., Sacchettini, J. C., Sauter, N. K., and Terwilliger, T. C. (2002) PHENIX: building new software for automated crystallographic structure determination. *Acta Crystallogr. D Biol. Crystallogr.* **58,** 1948–1954
44. Jones, T. A., Zou, J. Y., Cowan, S. W., and Kjeldgaard, M. (1991) Improved methods for building protein models in electron density maps and the location of errors in these models. *Acta Crystallogr. A* **47,** 110–119